Cancer Medicine Journal

Research Article | Vol 5 Issue S6

An Integrative Approach to Decipher the Role of OCT-1 in Imatinib Resistant Chronic Myeloid Leukemia

Krupa Shah[1], Saumya Patel[2], Rakesh Rawal[3*], Bhavesh Parekh[4] and Jyoti Bajaj Sawhney[5]

[1]*Department of Cancer Biology, The Gujarat Cancer & Research Institute (GCRI), Gujarat, India*

[2]*Department of Life Sciences, Gujarat University, Gujarat, India*

[3]*Department of Botany Bioinformatics and Climate Change Impacts Management, Gujarat University, Gujarat, India*

[4]*Department of Medical and Pediatric Oncology, The Gujarat Cancer and Research Institute (GCRI), Gujarat, India*

[5]*Department of Pathology, The Gujarat Cancer and Research Institute (GCRI), Gujarat, India*

Correspondence should be addressed to Rakesh Rawal, Department of Life Sciences, School of Sciences, Gujarat University, Ahmedabad-380009, Gujarat, India

Received: April 29, 2022; Accepted: May 24, 2022; Published: May 31, 2022

ABSTRACT

Resistance to tyrosine kinase inhibitors (TKIs) in chronic myeloid leukemia is multifactorial - multistep phenomenon may dependent or independent of BCR-ABL activity. An influx protein human organic cationic receptor-1 governs many CML related TKIs and associated with therapeutic resistance and response in CML. However, OCT-1 mediated drug uptake mode and intracellular retention in CML is not understood well. Hence, present study aims to explore the drug translocation mechanism through OCT-1 channel using structure-based computational approaches and correlate the observations with OCT-1 quantitative expression analysis in CML patients. Structure based computational analysis of OCT-1 transmembrane channel revealed most stable interaction with Imatinib at OCT-1 pore cavity as compared to other drug molecules. A significantly decreased OCT-1 expression in CML advanced phases and CD34+/CD38- cells, advocated Imatinib to impermeable and allow other molecules at OCT-1 pore cavity suggesting indirect prompting of BCR-ABL independent activity. Increased OCT-1 expression in Hydrea received patients confirms better penetration of Hydrea at the OCT-1 pore cavity. Hence, present study explored the mechanism of TKI selectivity through OCT-1 channel and OCT-1 attributed BCR-ABL independent drug resistance mechanisms to prognosticate the clinical relevance of OCT-1 as a potential therapeutic biomarker in CML patients for monitoring therapeutic response for better clinical management.

KEYWORDS

Organic cation transporter-1; Transmembrane channel; Tyrosine kinase inhibitors; Chronic myeloid leukemia; Drug resistance

INTRODUCTION

Chronic myeloid leukemia (CML) is a clonal myeloproliferative hematopoietic stem cell disorder characterized by unique chromosomal abnormality t(9;22)(q34;q11), caused the formation of BCR-ABL1 fusion gene with abnormal oncoprotein and enhanced tyrosine

Citation: Krupa Shah, An Integrative Approach to Decipher the Role of OCT-1 in Imatinib Resistant Chronic Myeloid Leukemia. Cancer Med J 5(S6): 69-83.

kinase activity, considered to be the pathogenic driver of CML multiphase progression [1,2]. However, since the last decades, advancement in targeting BCR-ABL1 tyrosine kinase inhibitors (TKIs) has completely modernized the era of CML treatment history over conventional therapy [3]. Though, treatment failure, loss of response and relapse owing to primary and secondary resistance has always been a major cause of concern in a proportion of patients accountable for chronic to blastic phase transformation leading to overall disease progression [4-43]. Disease progression due to phase transformation in CML is multistep- multifactorial phenomenon and may dependent or independent of BCR-ABL activity [7,8-14]. In CML, the function of efflux and influx transporters in maintaining the intracellular drug concentration through uptake and extrusion of TKIs has received much attention in recent years. Among all, transporters, an important human Organic Cation Transporter-1 (hOCT-1), a solute carrier-major channel influx protein controls the uptake of many chemotherapeutic cationic drugs, including imatinib, and aberrant OCT-1 expression arbitrate the Imatinib transportation uptake rate, intracellular concentration and overall therapeutic response in CML patients [10,15]. Several authors have demonstrated the association between OCT-1 expression and Imatinib response in early-stage CML patients, suggesting that patients with high OCT-1 expression activity attained prompt progression-free and overall survival, especially those received Imatinib as front-line therapy [9-11,13-15,20]. While patients with low OCT-1 expression activity reported to have a high risk of developing resistance and disease progression [15-18]. Despite cumulative experimental evidence demonstrating the association between the functional activity of OCT-1 and Imatinib, the interaction of OCT-1 with drug selection and intracellular delivery across the membrane is not yet clearly understood and further needs to be explored in detail [19]. In addition, the lack of or very limited comprehensively modelled OCT-1 protein structure information expedited the prediction of the OCT-1 modeled structure and transmembrane channel. Therefore, present study aims to predict the homology modeling of OCT-1 protein structure and OCT-1 transporter channel using various computational approaches. Moreover, comprehensive molecular docking and simulation analysis was performed to identify the best TKI interaction at the OCT-1 pore cavity compared to other CML TKIs. Further, in order to confirm the OCT-1 as a potential influx protein responsible for activation of BCR-ABL independent mechanisms, computationally derived data were correlated with the quantitative expression of OCT-1 in CML patients and CML +/ CD38-stem cells.

MATERAILS AND METHOD

Patients Collection and Selection Criteria

Total 120 CML samples from each phase chronic (N = 30), accelerated (N = 30), and Blastic crisis (N = 30), from the year 2011-2015 were collected from Gujarat Cancer & Research Institute, Gujarat, India. Of the collected samples, N = 58 were received Imatinib, N = 32 received Hydrea and N = 30 received Imatinib + Hydrea as therapy. Prior informed consent and institutional ethical approval were obtained before sample collection. Following criteria were considered for the patient selection: If patient has not received any therapy at time of collection considered as untreated samples and those who fails to achieve an either hematological, cytogenetic, or molecular response also included as follow up samples. NCCN guidelines were followed for the patient's response and resistance criteria. The patient's baseline clinico-pathological and demographic details such as age, sex, spleen size, WBC count, differential count, platelet count, and peripheral blasts percentage were recorded. Median range of patient's age was 39 (18 years - 70 years), splenomegaly size 17 (11 cm - 84.7 cm), Basophils count 3 (0 cells/µl - 20 cells/µl), Eosinophil count 3 (0.1 cells/µl - 16 cells/µl), W.B.C. count 146000 (2900 count/µl - 754800 count/µl), Platelet

count 373000 (6600 count/µl - 754800 count/µl), and Peripheral blast 3 (1%-87%).

Quantitative Reverse Transcriptase PCR (qRT-PCR)

Mononuclear cells were acquired by ficoll (Histopaq-1077, Sigma) density gradient centrifugation from collected bone marrow and blood samples followed by positive selection and enrichment of CML CD34+/ CD38- subpopulation of cells through midi MACs immuno-magnetic separation (Miltenyi Biotech, Germany). Total RNA was extracted from Nucleospin total RNA isolation kit (Macherey-Nagel) followed by cDNA synthesis using iScript cDNA synthesis kit (Bio-Rad) as per manufacture instructions. qRT-PCR was performed using SYBR green based Brilliant III Ultra-Fast qRT-PCR 2 × Master mix (Agilent Technology), OCT-1 primers (F: 5'-CTG AGC TGT ACC CCA CAT TCG-3', R: 5'-CCA ACA CCG CAA ACA AAA TGA-3') and 20 ng of cDNA as an initial template on ARIAMx system (Agilent Systems, USA). Following thermal cycling condition was set to amplify the OCT-1 region: Hot start activation at 95°C for 3 minutes, followed by 40 cycles of, denaturation at 95°C of 5 seconds, annealing at 60°C for 10 seconds and reaction hold at 4°C. GAPDH was used as a reference transcript for calculating the fold change expression. Each experimental reaction was set up in triplicate with no template control for expression analysis. Threshold (Ct) value generated after an experimental run was used to calculate the fold difference between the target gene and reference gene using the 2^ΔΔct method. To avoid the sample heterogeneity, fold change of bone marrow and blood samples were analyzed against naïve stem cells and MNCs, respectively.

Statistical Analysis

Two-tailed Student t-tests were used for statistical analysis. The difference was considered statistically significant when the P-value is less than 0.05. The data represented as mean ± SD of the number of the determinations and analyzed by SPSS software version 20.

Computational Structural Molecular Modeling and Transmembrane Helices Prediction of OCT-1

Computer-aided homology modeling of OCT-1 was performed after retrieval of OCT-1 (O15245: S22A1_HUMAN) protein sequence from UniProtKB/Swiss-Prot database (The UniProt Consortium, 2012) [26,27]. A Sequence homology search was carried out with the BLASTP server, followed by a prediction of OCT-1 homology structure with Phyre2 Server [24]. The BLASTP server uses the best five iterative runs from databases and identifies the best sequence homology of the queried OCT-1 protein sequence, which was subjected to the Phyre2 server to build OCT-1 homology modelled structure. Three states of the secondary structure, alpha-helix (H), beta-strand (E - for extended), and coil (C) prediction of the generated model structure were confirmed using Psi-Pred [21], Jnet [25], and SSPro [29] independent programs that output the information along with confidence value in the form of consensus. The generated OCT-1 model was energy minimized using YASARA energy minimization server [34] and subjected to the TMHMM 2.0 program for transmembrane helices predictions [30].

OCT-1 Model Quality and Accuracy

The stereo chemical characteristics of the predicted modeled structure were confirmed with the Ramachandran plot [33] using an online Structure Analysis and Verification Server (SAVES) (http://nihserver.mbi.ucla.edu/SAVES). The identification of mistraced atomic coordinates, the accuracy of the bond length accuracy, the correctness of the amino acid chirality and quality factor of the verified protein structure were further evaluated with ERRAT2 server [22,23]. Subsequently, the OCT-1 channel prediction, characterization and complete structural organization such

as pore diameter profiles, pore-lining residues, pore size, and shape were determined with the Pore-Walker program [32].

Molecular Docking Experiment Settings

Total six drug molecules Imatinib, Nilotinib, Dasatinib, Ponatinib, Hydrea and Diclofenac retrieved from PUBCHEM database and subjected to AMBER03 force field-based energy minimization on the YASARA platform to in order to obtain a stable conformation of the structures. Before Docking, the homology-modeled OCT-1 protein structure was preprocessed to remove water molecules and encompass explicit polar hydrogen atoms as well as electrostatics using Autodock tools 4. For binding site generation, torsional restrained were kept flexible in ordered to attain the favorable binding conformation. Finally, the docking on Autodock 4.2 was performed by assigning the grid size 48 × 62 × 62 XYZ points with a grid spacing of 0.375 Å and setting the grid center with a dimension of x = 50.19 Å, y = 39.05 Å, and z = 36.55 Å [31]. Rest optimization parameters were set to standard. To identify the best ligand- protein position, an active site-directed docking simulation was performed, which was clustered based on the RMSD value and binding free energy. Finally, top-scoring binding conformers were considered for ligand-protein interactions and were selected for further refinement using MD simulation.

Molecular Dynamics Studies of OCT-1

A structure-based 100 ns molecular simulation was set up to investigate the dynamic behavior of the docked protein-ligand complexes on the YASARA platform. Before simulation, complexes were subjected to energy minimization in order to determine to the atomic coordinates of the protein structure. Simulation complexes were embedded with Palmitoyl Ethanol Amide lipids (237 molecules) - water (7537 molecules) membrane, with the OCT-1 transmembrane region occupying the lipid membrane and its cytosolic regions being solvated by water molecules. Rest of simulation assisted with transferable intermolecular potential 3 points (TIP3P) water molecules (density 0.997 g L^{-1}), AMBER03 force field, temperature 298 K, and pH 7.4 [36]. Periodic boundaries were defined with a cell extension of 10Å, the system neutralization was carried out with 0.9% NaCl and energy minimization was performed with the steepest gradient approach (5000 cycles) followed by the simulated annealing method. Subsequently, equilibration was performed by considering harmonic restraints on all heavy atoms of the protein–ligand complex (force constant= 1000 kJ mol^{-1} nm^{-2}). Particle mesh Ewald method was employed to calculate the long-range electrostatics with a cutoff of 10 Å [35,37]. Simulation snapshots were taken at every 10,000 simulations with a period of 25 ps (One simulation time step at 2.5 fs, i.e. 10,000 × 2.5 = 25 ps). The generated RMSD (Root Mean Square Deviation) and RMSF (Root Mean Square Fluctuation) trajectories were analyzed for the structural stability of the docked protein-ligand complexes.

RESULTS

Template Selection and Homology Modelling

The three- dimensional model of the OCT-1 protein was predicted by employing OCT-1 (ID O15245) protein sequence to PSI-BLAST to identify the best template against the query sequence. Based on the Position Scoring Matrix System (PSSM), PSI-BLAST identified the sequence similarity with domain of general substrate transporters - Major Facilitator Super Domain (MSF) in different organisms against OCT-1 query sequence. Identified templates demonstrated E-value in the range from 2 e-061 to 5.9 e-07 with 100% precision, accuracy and high sequence convergence, were therefore selected for the 3D model generation. The secondary structure prediction was performed using PSI-Pred, Jnet, and SSpro which was further implemented in Phyre2 server to in order

to generate a consensus across the sequence window and resulting values (>5) further substantiate the confidence of the model structure, from the seed for the model was developed.

Transmembrane Helices Prediction and Model Validation

An online server TMHMM v 2.0 was used to predict trans membrane helices, which identified putative 12 helices with a maximum residual length of 6 amino acids and 12 amino acids for beta sheets and alpha helices, respectively. The OCT-1 protein consists of 554 amino acids, with an expected number of amino acids involved in helices prediction are 255.20728 of the input OCT-1 sequence (Figure 1).

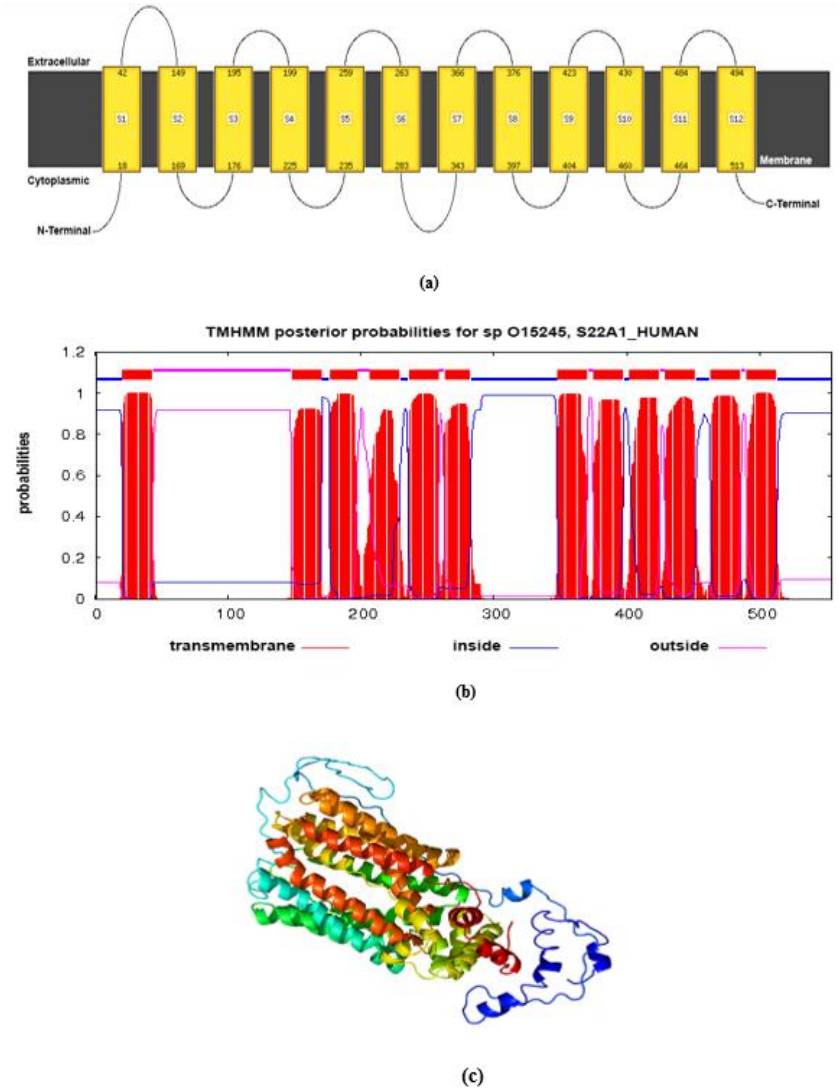

Figure 1: Predicted Homology model of the OCT-1 Protein Structure. **A)** OCT-1 model contains 12 transmembrane helices (THM). Both C- terminal and N-terminal is inside the cells; **B)** TMHMM predicted 12 putative TM helices in OCT-1 structure; **C)** Overall tertiary structure of OCT-1.

The structural quality check of the predicted protein structure revealed the overall probability values of 0.91 and all posterior probability values close to 1for the transmembrane helices. In addition, the Ramachandran plot analysis exhibited the presence of 97.7% of all residues in a core area (phi-psi), with the exception of Glycine residue, which was preset in the disallowed region (Figure 2A and Figure 2B). The overall structure quality

was predicted by the ERRAT2 plot server was as just as reliable at 67.82% as a reliable model with an overall quality factor of about 91% with resolutions of 2.5 Å to 3 Å (Figure 2C and Figure 2D).

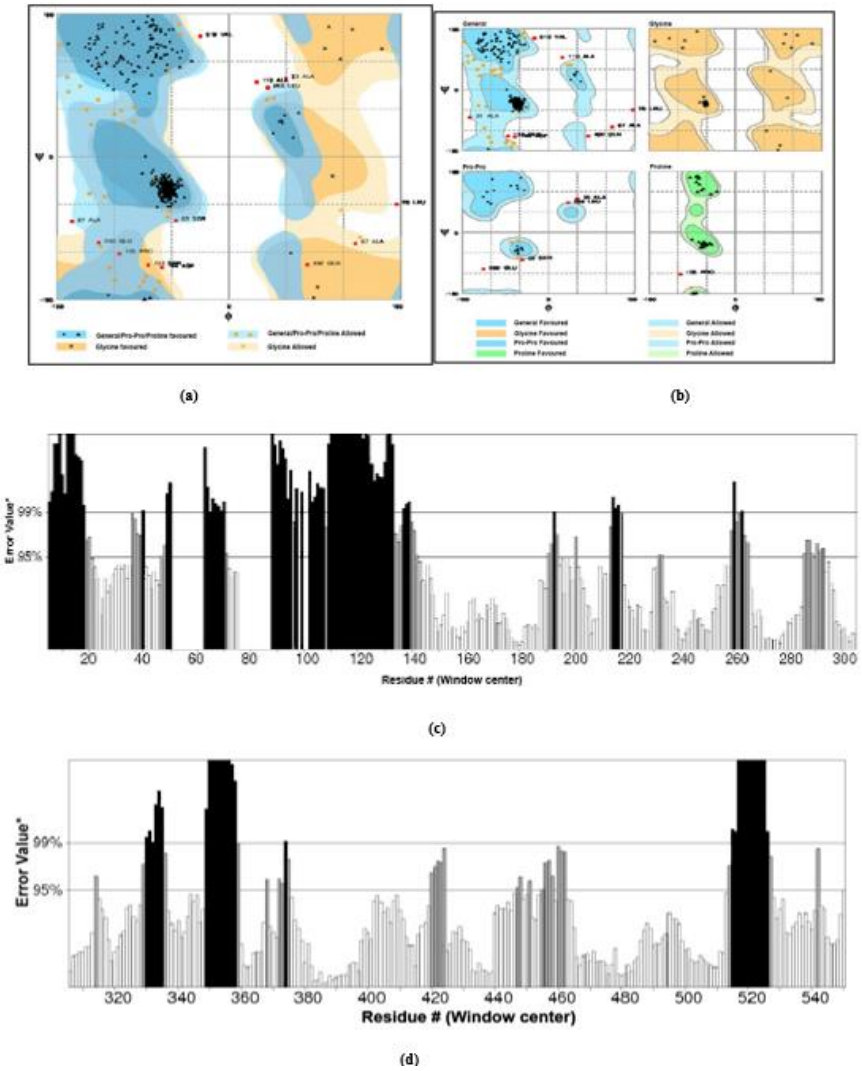

Figure 2: Validation and Quality check of the predicted Homology Build of OCT-1 Protein Structure. **A & B)** Ramachandran Plot for the OCT-1 structure. It scores 97.7 % for the percentage of residues residing in the most favorable region, with the exception of amino acids excluding Gly and pro-occupied in the disallowed region. **C & D)** ERRAT analysis of OCT-1 structure. Black bars indicate a misfolded region, grey bars represent an error between 95% and 99%, while white bars indicate an area with low error rate.

OCT-1 Transmembrane Channel Prediction

A comprehensive structural characterization of OCT-1 transmembrane channel prediction was accomplished through the Pore Walker program. Initially, the pore axis demarcation was done by sectioning the protein structure cutting along the XY- plane, which defines the putative pore-lining residues (Color Orange) and atoms (Color Blue) in proximity to the pore axis and also detects the cavity pore center at 3 Å (Red Spheres) from given pore heights. Further, throughout the pore axis from negative to positive coordinate attained pore shape is UDSDUS (from top to bottom, S denotes cylinder, and D and U represent decreasing and increasing conical frustum, respectively), defined in two dimensional as a stack of building blocks (Figure 3A and Figure 3B). The diameter profile of the pore at 3 Å steps corresponding to the pore shape in the pore channel is also analyzed. Moreover, the cavity with the biggest pore sphere "center" was identified along the channel at 1 Å steps (Figure 3C and Figure 3D). Besides,

the regularity of the pore cavity was verified by the presence of consecutive straight lines and wiggly lines in the channel area, which authenticate the position of the pore center at 1 Å along the pore axis. The presence of straight lines indicated the low RMSD area and curved lines represented the highly spread pore area. Pore diameter profile at 1 Å steps conforming the pore shape in the pore channel was also calculated (Figure 3E and Figure 3F). Further, for a better understanding of the pore channel, horizontal sections of the protein structure were produced perpendicular to the pore axis, which characterizes the pore details, negative and positive coordinates along the pore axis from the bottom and top view, respectively (Figure 3G - Figure I).

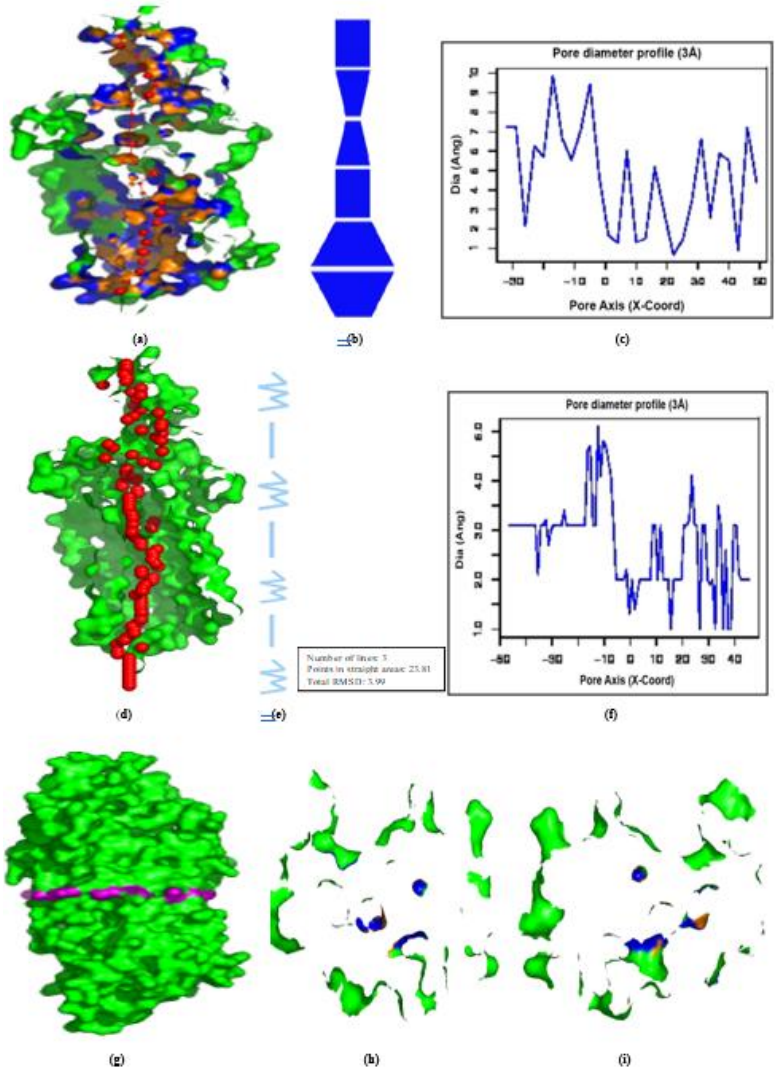

Figure 3: Structural and functional characterization of transmembrane channel of the homology modeled OCT-1 structure. **A)** Visualization of the XY- plane of the protein structure defining pore-lining residues and pore centers at 3Å steps of the pore section, where, x-axis denotes the pore x-axis and Y-coordinate >0 is displayed. **B)** Representation of the pore shape along the pore line in the 2D image. **C)** Pore diameter profile at 3 Å, where X-axis denoting the position along the pore axis and Y-axis denoting pore diameter value in Å. **D)** A visualization of the Pore section defining the position of the largest pore center at 1Å. **E)** Illustration of the regularity of the pore cavity with straight and curved lines representing channel areas. **F)** The pore diameter profile at 1 Å, where the X-axis denotes the position along the pore axis and Y-axis denotes the pore diameter value in Å. **G)** Horizontal section of the pore (purple color) at the pore heights. **H)** Horizontal view from the bottom representing most negative coordinates. **I)** Horizontal view from the top defining most positive coordinates.

Identification of Top Ligand-Protein Conformers and Molecular Simulations

Docking simulation identifies the best protein-ligand conformers based on their binding free energy and interacting residues. Docking result depicted that out of 6 docked ligands, Imatinib ranked top with a higher binding affinity (10.1180 kcal/mol), then Ponatinib (10.0630 kcal/mol), Nilotinib (9.2960 kcal/mol), Dasatinib (8.9090 kcal/mol), Diclofenac (7.5690 kcal/mol) and Hydroxyurea revealed less binding affinity (3.8340 kcal/mol) at OCT-1 binding site. In addition, the difference in interacting residues between protein-ligand complexes was also analyzed. As listed in Table 1; OCT-1 interacts with docked Imatinib molecules with residue numbers Ser 133, Ile 134, Gln152, Leu155, Phe159, Asn186, Met193, Arg206, Gln209, Val212, Ser213, Asn216, Trp217, Phe 244, Leu248, Leu251, Thr 252, Ala255, Val268, Leu360, Tyr361, Leu364, and Tyr376.

Drug Molecules	Type of Strain Amino Acid Interactions	Docking Energy (Kcal/mol)
Imatinib	SER 133 ILE 134 GLN152 LEU155 PHE159 ASN 186 MET193 ARG206 GLN209 VAL212 SER213 ASN216 TRP217 PHE 244 LEU248 LEU251 THR 252 ALA255 VAL268 LEU360 TYR361 LEU364 TYR376	10.1180
Ponatinib	SER 133 ILE 134 LEU 155 PHE159 ARG 206 SER 213 TRP217 GLN241 PHE244 LEU248 LEU 251 THR252 ALA255 TRP 261 LEU353 THR356 LEU 360 TYR 361 PHE 379 ILE 446 CYS 473 GLY477	10.0630
Nilotinib	LEU 179 GLY 220 LEU 223 ILE 224 PHE 227 VAL 228 VAL 236 MET 239 TYR 240 ALA 243 PHE 275 TYR 278 TYR 279 VAL 282 PRO 283	9.2960
Dasatinib	LEU 179 VAL 183 ASN 186 GLN 209 ASN 216 GLY 220 LEU 223 ILE 224 PHE 227 VAL 236 MET 239 TYR 240 LEU 251 VAL 268 PRO 271 THR 272 PHE 275 TYR 279 VAL 282	8.9090
Diclofenac	ILE 134 GLU 137 PHE 138 VAL 141 CYS 142 LEU 148 PHE 151 MET 202 ALA 255 HIS 260 TRP 261 LEU 264 GLN 265 LEU 266	7.5690
Hydroxyurea	ASN 71 TYR 72 THR 73 VAL 74 SER 230 GLY 231 GLY 518 VAL 519 ALA 520	3.8340

Table 1: Docking result of OCT-1 with drug molecules- binding energy and interacting residues.

Further, to understand the "local" structural stability at the residual level of the docked protein - ligands; trajectories generated by molecular simulations were analyzed. Since Imatinib showed the highest binding affinity as compared to other docked complexes, we further proceeded our analysis with only OCT1-Imatinib complex for structural stability analysis. After a long 50ns MD simulation of OCT-1 bound in complex with Imatinib indicated that docked complex started to be stabilized at 500 ps (peak - 870070 kJ/mol) and achieved the steady phase for the rest of simulation period (500 ps - 10000 ps) (Table 2) which clearly stated that Imatinib strongly hold the OCT-1 pore cavity as compared to other docked drug molecules. Interestingly, almost similar trend was observed for other energy contributors such as bond, angle, dihedral angle, planarity, coulombic charge, and vander Waals, which was highest at 500 ps, stabilize and attain the plateau phase for the rest simulation period [Figure 4]. Analysis of initial and sfinal (100 ns) structure superimposition of Imatinib bound complex revealed that overall structure is well stabilized in the system with minimal fluctuations occurred in their extremities proving it the most stable complex in the OCT-1 channel residue.

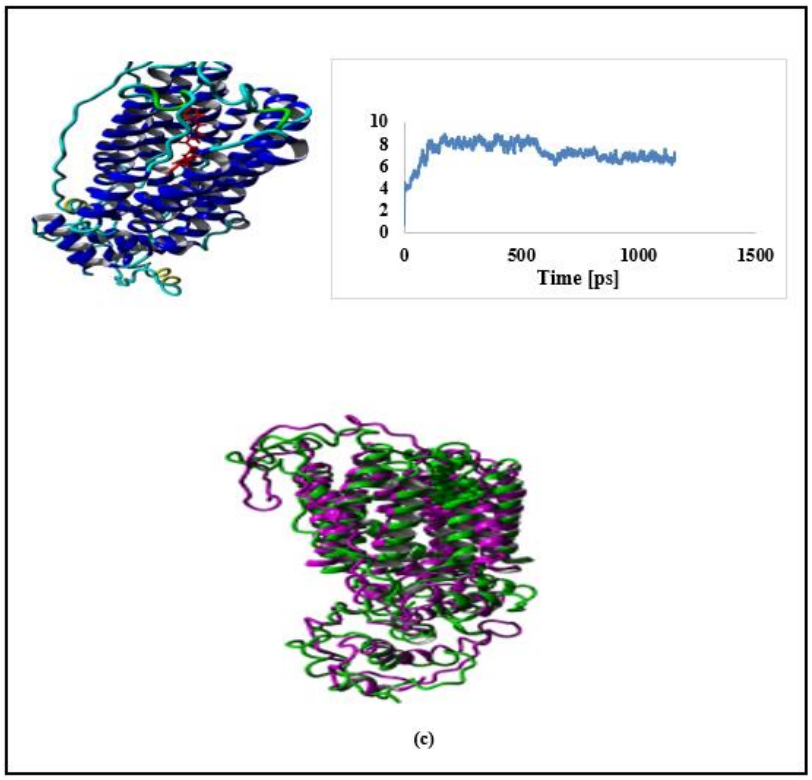

Figure 4: Representation of Docking and Molecular Simulation Analysis of Homology modeled OCT-1 protein- Imatinib complex. **A)** Docking conformers of OCT-1- Imatinib complex at the OCT-1 binding Site; **B)** RMSD trajectory of OCT-1-Imatinib complex after MD simulation; **C)** Snapshot of structure superimposition of OCT-1-Imatinib complex with initial and after MD simulation at 100ns.

OCT-1	Time (ps)	Energy (kJ/mol)	Bond	Angle	Dihedral	Planarity	Coulomb	VdW	RMSDs
Imatinib	100	-879186	101744.4	92380.32	217611.8	1080.899	-13890 84	97080.96	7.282

Table 2: Molecular dynamics interaction - energy profile of OCT-1-imatinib complex.

Assessment of OCT-1 Expression in CML Phases, Received Treatments and in Blood and Bone Marrow Samples

To corroborate the *in-silico* analysis, we evaluated the OCT-1 fold change expression in isolated CML MNCs, CML stem CD34+/ CD38- populations, in patients receiving different therapeutic treatments as well as in blood and bone marrow samples. When OCT-1 expression was assessed in different CML phases, no major fold change expression was obtained between at diagnosis and chronic phase patient. However, a decreased fold change expression was observed as the disease progressed to blastic crisis and a significant OCT-1 down regulation was noticed when compared between chronic and accelerated phase (P-value: 0.04) and blastic phase (P-value: 0.01) (Figure 5A and Figure 5B). When OCT-1 expression was assessed in isolated CML CD34+/CD38- specific cell population, a significant down- regulation of OCT-1 was observed as compared to CML mononuclear cells (P-value: <0.0001) (Figure 5A). When OCT-1 expression was evaluated between Imatinib, Hydrea and Imatinib + Hydrea received patients, a decreased fold change expression was reported in Imatinib received patients as compared to Hydrea standalone and in a combination of treatment. However, no major fold change expression was observed between Hydrea standalone and a combination of Imatinib + Hydrea received patients (Figure 5C). When the fold

change expression was measured between bone marrow and blood samples, bone marrow samples showed a significantly high OCT-1 expression as compared to blood samples (P-value: 0.02) (Figure 5D).

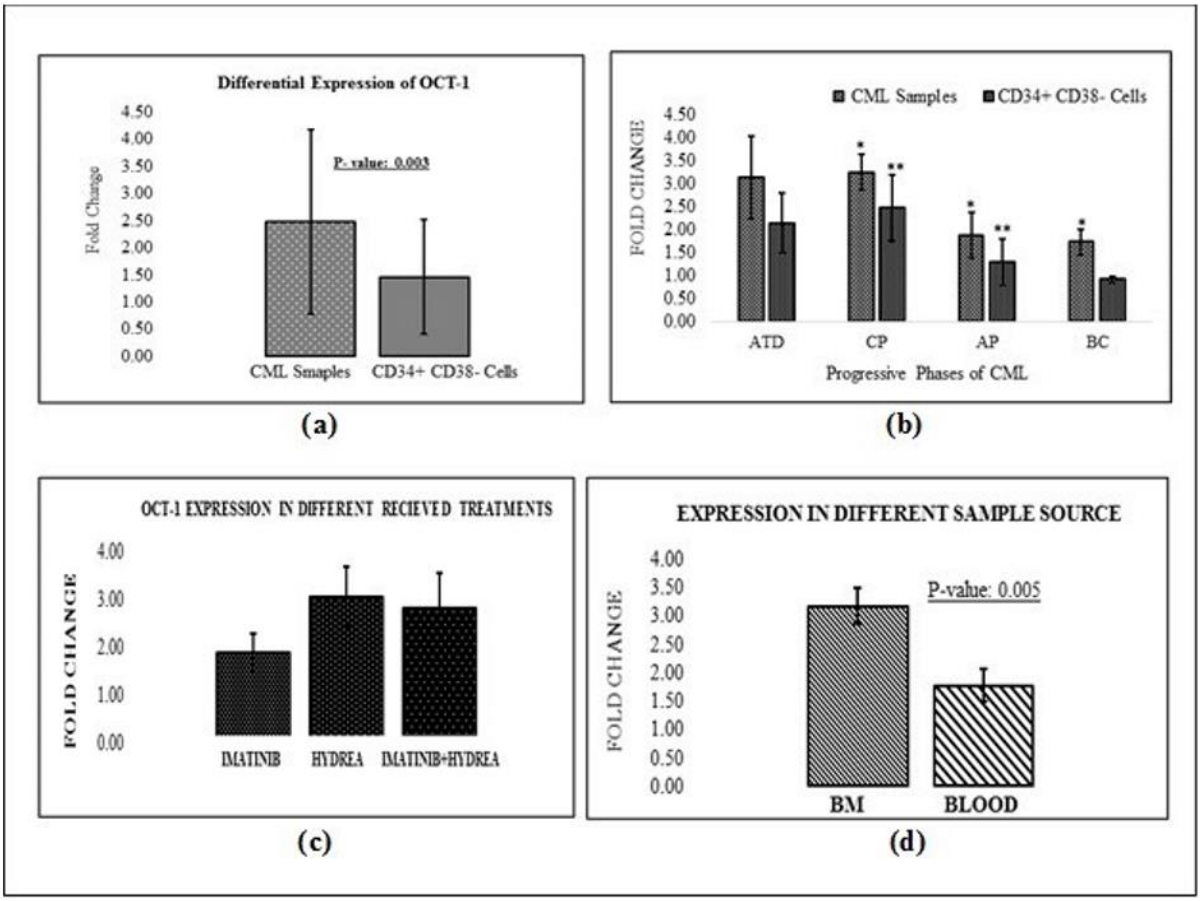

Figure 5: Differential expression OCT-1 assessed by qRT-PCR in CML patients and CML stem cells. **A)** Bar graph shows the OCT-1 fold change expression between CML samples and CML CD34+/CD38- population (P-value: 0.003). **B)** OCT-1 expression in progressive CML phases between CML samples and isolated CD34+/CD38- population. Data are mean ± SD. *P-value <0.05 and **P-value <0.005. **C)** Fold change expression level of OCT-1 response to received Imatinib, Hydrea, and a combination of Imatinib+ Hydrea therapy. **D)** Bar graphs represent the OCT-1 expression level in Bone marrow and Blood samples (P-value: 0.005).

DISCUSSION

Despite the tremendous success of Imatinib, drug resistance in CML and transition from CP to BC via AP is a multistep inter-correlated molecular event that may or may not be dependent on BCR-ABL activity [4-7]. Altered expression of influx transporter OCT-1, which is involved in the uptake of many chemotherapeutic drugs, is reported to influence the therapeutic response in CML patients [9,10]. Molecular insight on ligand recognition by OCT-1 and the mechanisms by which it mediates the translocation of the molecules into the cells is of great interest but not yet well understood. Therefore, in the present study, we attempted to probe the unexplored drug-transporter mechanism using various computer-aided approaches and correlate the data with OCT-1 expression in CML MNCs and stem cells.

Increasing efforts to understand the interaction between the OCT-1 transporter and substrate in order to identify the contact residues based on the hypothesized 3D structure have been reported. One of the major limitations of these studies, however, lies in the fact that computationally generated homology model shared low sequence

resemblance with human OCT-1 due to their difference in origin [41,42]. Recently, a group of authors Popp et.al. generated an OCT-1 homology model in an occluded state from a known available MFS transporter of eukaryotic origin with a relative sequence homology of 40% with the hOCT-1 [43]. It could reliably predict the critical amino acid residues involved in the transporter and substrate interaction. As we had limited understanding of crystal structure of the OCT-1 protein, one of the major challenges was to generate a complete 3D structure. Therefore, in the current study, we performed template-based homology modeling to predict three-dimensional structure of the OCT-1 protein with high sequence similarity and accuracy, which is clearly shown by Ramachandran plot analysis.

Another important aspect of this study is to predict the structural and functional characterization of the homology modeled OCT-1 protein transmembrane channel, which was achieved by a fully automated Pore walker program. Predicted pore axis, cutting along the XY-plane of the protein structure confirms that path the ligand takes through the transmembrane channel is linear and the pore is perpendicularly passes through the membrane. Moreover, pore descriptors analysis such as regularity of the pore cavity, pore shape, position of the pore center, atoms, and corresponding residues along the pore line further substantiates the channel organization and functionality towards ligands that run through the transmembrane plane. To the best of our knowledge, we believe that this is the first primary study that comprehensively predict the functional insight of the OCT-1 transmembrane channel to comprehend the ligand pathway along the pore channel. Another crucial aspect of predicted transmembrane channel is to identification of the contacting amino acid residues throughout the OCT-1 pore channel. Our extensive analysis of the predicted transmembrane channel revealed several amino acids within the OCT-1 channel pore indicated as red dots in homology model predicted protein structure, which are anticipated to directly contribute to substrate specificity. Further, in ordered to identify the best drug selectivity and binding efficiency towards the OCT-1 pore cavity, extensive molecular docking and long-term simulation analysis was also carried out. Our ligand-protein docking analysis revealed highest binding affinity with Imatinib at OCT-1 binding site and confirms the OCT-1 selectivity towards Imatinib as compared to other drug molecules used in the regimen. Additionally, post-docked structure-based molecular dynamic simulation trajectory analysis of OCT-1- Imatinib bound complex (100 ns) started to attained equilibrium at 500 ps and remains stable throughout the simulation trajectory, which further indicates a stable hold of Imatinib at OCT-1 binding site. Our observations authenticate the OCT-1 selectivity towards Imatinib, rendering the smoothest path of Imatinib to run along the OCT-1 pore channel and makes it entry to the cells more permeable as compared to other docked drug molecules.

Docking analysis with other docked TKIs demonstrated that, the binding affinity of Ponatinib with OCT-1 is comparable to that of Imatinib and, interestingly both share some common interacting amino acid residues in the OCT-1 cavity, suggesting a possible role for these residues for TKI selectivity by OCT-1. The binding affinity of Dasatinib, and Nilotinib with OCT-1, is less as compared to Imatinib and Ponatinib, which corroborate with published in-vitro results indicating passive uptake of these drugs regardless of OCT-1 activity [38-40]. Therefore, selection of these drugs may be reserved for patients showing low OCT-1 expression during therapy decision making.

Several reports linked conflicting observations on OCT-1 mediated uptake of Imatinib, and to date no broad consensus has emerged. However, earlier studies have

demonstrated association of OCT-1 functional activity in predicting clinical response in CML risk stratification [15-17]. Therefore, in the present study, to confirm the in-silico results, OCT-1 quantitative expression analysis of OCT-1 was performed to predict the OCT-1 mediated therapeutic response and resistance in CML patients. We observed a significant down regulation of OCT-1 expression in progressive phases (CP>AP>BC), which is consistent with previous reports. Decreased OCT-1 expression in advanced phases indicates the lower uptake of Imatinib into the cells thus unable to achieve optimum lethal concentration in CML cells. Furthermore, a reduced expression of OCT-1 in immuno-magnetically sorted CD34+ CD38- Ph+ CML stem cells as compared to patient's MNC samples from patients suggested an inherent potential of these stem cells for therapy resistance. It can be assumed that a low uptake of Imatinib may favour the other molecules to enter via passive mechanism due to reduced OCT-1 expression on CML cells. In addition, high OCT-1 expression in patients receiving Hydrea standalone or in combination with Imatinib confirms the better penetration of hydrea and is suggestive of the role of hydrea as inducer of OCT-1.

CONCLUSION

Drug resistance in CML is a sequential transition from CP to BC via AP is multifactorial and involves several molecular alterations independent of BCR-ABL expression. Proposed new approach in our study is the first step in understanding the selectivity and specificity of OCT-1 towards substrate drugs. We therefore believe that an in-silico analysis of OCT-1 interaction with different drug molecules can provide a better insight into the ligand binding and translocation through the OCT-1 pore channel. Decreased OCT-1 expression in CML advance phases and in CML stem cell populations indicates an inherent potential of these cells to develop therapeutic resistance. Increased expression of OCT-1 in patients treated with Hydrea alone or in combination with Imatinib suggested that Hydrea being a small molecule exhibit better penetration into the OCT-1 pore cavity compared to other TKIs. Therefore, inclusion of Hydrea before initiation of Imatinib may be a favorable protocol than Imatinib or Hydrea alone. Moreover, we believed that approach proposed in our study is the first step towards enhancing the understanding of the activation of BCR-ABL independent mechanism via plausible involvement of OCT-1 could be act as a potentially clinically relevant biomarker for predicting drug resistance in CML patients. However, it further required correlation with drug influx transporters to predict complete TKI response, resistance and disease monitoring.

ACKNOWLEDGEMENT

KRP acknowledges Indian Council of Medical Research (ICMR- F.No.5/4/13/2012-RMC) and Gujarat State Biotechnology Mission (GSBTM-FAP/167/13) for funding the project, SKP acknowledges Scientific and Engineering Research Board, Dept. of Science and Technology, Government of India for National Postdoctoral Fellowship (N-PDF) (Grant: PDF/2015/000328).

AUTHORS CONTRIBUTION

Conceptualization: Krupa Shah, Saumya Patel, Rakesh Rawal, Methodology, Analysis & Interpretation of the Data: Krupa Shah, Saumya Patel, Supervision: Dr. Bhavesh Parekh, Dr. Jyoti Bajaj Sawhney, Dr. Rakesh Rawal, Original Draft Preparation: Krupa Shah, Revising the Manuscript: Krupa Shah, Rakesh Rawal, Final Approval: Rakesh Rawal. All authors read, agreed and approved the manuscript.

COMPETING INTEREST

The author declared that there is no potential conflict of interest.

REFERENCES

1. Apperley JF (2007) Part I: Mechanisms of resistance to imatinib in chronic myeloid leukaemia. The Lancet Oncology 8(11): 1018-1029.
2. Cowan-Jacob SW, Guez V, Fendrich G, et al. (2004) Imatinib (STI571) resistance in chronic myelogenous leukemia: Molecular basis of the underlying mechanisms and potential strategies for treatment. Mini Reviews in Medicinal Chemistry 4(3): 285-299.
3. Altschul SF, Madden TL, Schäffer AA, et al. (1997) Gapped BLAST and PSI-BLAST: A new generation of protein database search programs. Nucleic Acids Research 25(17): 3389-3402.
4. Ali MA (2016) Chronic myeloid leukemia in the era of tyrosine kinase inhibitors: An evolving paradigm of molecularly targeted therapy. Molecular Diagnosis & Therapy 20(4): 315-333.
5. Donato NJ, Wu JY, Stapley J, et al. (2004) Imatinib mesylate resistance through BCR-ABL independence in chronic myelogenous leukemia. Cancer Research 64(2): 672-677.
6. Shah K, Parikh S, Rawal R (2016) Tyrosine kinase inhibitors in ph+ chronic myeloid leukemia therapy: A review. Asian Pacific Journal of Cancer Prevention 17(7): 3025-3033.
7. O'hare T, Zabriskie MS, Eiring AM, et al. (2012) Pushing the limits of targeted therapy in chronic myeloid leukaemia. Nature Reviews Cancer 12(8): 513-526.
8. Bavaro L, Martelli M, Cavo M, et al. (2019) Mechanisms of disease progression and resistance to tyrosine kinase inhibitor therapy in chronic myeloid leukemia: An update. International Journal of Molecular Sciences 20(24): 6141.
9. Brosseau N, Ramotar D (2019) The human organic cation transporter OCT1 and its role as a target for drug responses. Drug Metabolism Reviews 51(4): 389-407.
10. Crossman LC, Druker BJ, Deininger MW, et al. (2005) hOCT 1 and resistance to imatinib. Blood 106(3): 1133-1134.
11. Koepsell H (2015) Role of organic cation transporters in drug-drug interaction. Expert Opinion on Drug Metabolism & Toxicology 11(10): 1619-1633.
12. Fromm MF (2015) Transporters and drug–drug interactions: Important determinants of drug disposition and effects. Toxicology Letters 2(238): S49.
13. Koren-Michowitz M, Buzaglo Z, Ribakovsky E, et al. (2014) OCT 1 genetic variants are associated with long term outcomes in imatinib treated chronic myeloid leukemia patients. European Journal of Haematology 92(4): 283-288.
14. Walz C, Sattler M (2006) Novel targeted therapies to overcome imatinib mesylate resistance in chronic myeloid leukemia (CML). Critical Reviews in Oncology/Hematology 57(2): 145-164.
15. Watkins DB, Hughes TP, White DL (2015) OCT1 and imatinib transport in CML: Is it clinically relevant?. Leukemia 29(10): 1960-1969.
16. White DL, Saunders VA, Dang P, et al. (2007) Most CML patients who have a suboptimal response to imatinib have low OCT-1 activity: Higher doses of imatinib may overcome the negative impact of low OCT-1 activity. Blood, The Journal of the American Society of Hematology 110(12): 4064-4072.

17. White DL, Saunders VA, Dang P, et al. (2006) OCT-1-mediated influx is a key determinant of the intracellular uptake of imatinib but not nilotinib (AMN107): Reduced OCT-1 activity is the cause of low in vitro sensitivity to imatinib. Blood 108(2): 697-704.
18. Kim YK, Lee SS, Jeong SH, et al. (2014) OCT-1, ABCB1, and ABCG2 expression in imatinib-resistant chronic myeloid leukemia treated with dasatinib or nilotinib. Chonnam Medical Journal 50(3): 102-111.
19. Nies AT, Schaeffeler E, van der Kuip H, et al. (2014) Cellular uptake of imatinib into leukemic cells is independent of human organic cation transporter 1 (OCT1). Clinical Cancer Research 20(4): 985-994.
20. Wang Y, Xiao J, Suzek TO, et al. (2009) PubChem: A public information system for analyzing bioactivities of small molecules. Nucleic Acids Research 37(suppl_2): W623-W633.
21. Buchan DW, Ward SM, Lobley AE, et al. (2010) Protein annotation and modelling servers at University College London. Nucleic Acids Research 38(suppl_2): W563-W568.
22. Colovos C, Yeates TO (1993) Verification of protein structures: Patterns of nonbonded atomic interactions. Protein Science 2(9): 1511-1519.
23. Gasteiger J, Marsili M (1980) Iterative partial equalization of orbital electronegativity - a rapid access to atomic charges. Tetrahedron 36(22): 3219-3228.
24. Kelley LA, Sternberg MJ (2009) Protein structure prediction on the Web: A case study using the Phyre server. Nature Protocols 4(3): 363-371.
25. Cuff JA, Barton GJ (2000) Application of multiple sequence alignment profiles to improve protein secondary structure prediction. Proteins: Structure, Function, and Bioinformatics 40(3): 502-511.
26. Murzin AG, Brenner SE, Hubbard T, et al. (1995) SCOP: A structural classification of proteins database for the investigation of sequences and structures. Journal of Molecular Biology 247(4): 536-540.
27. UniProt Consortium (2018) UniProt: The universal protein knowledgebase. Nucleic Acids Research 46(5): 2699.
28. Bernstein FC, Koetzle TF, Williams GJ, et al. (1977) The protein data bank: A computer-based archival file for macromolecular structures. Journal of Molecular Biology 112(3): 535-542.
29. Pollastri G, Przybylski D, Rost B, et al. (2002) Improving the prediction of protein secondary structure in three and eight classes using recurrent neural networks and profiles. Proteins: Structure, Function, and Bioinformatics 47(2): 228-235.
30. Krogh A, Larsson B, Von Heijne G, et al. (2001) Predicting transmembrane protein topology with a hidden Markov model: Application to complete genomes. Journal of Molecular Biology 305(3): 567-580.
31. Morris GM, Huey R, Lindstrom W, et al. (2009) AutoDock4 and AutoDockTools4: Automated docking with selective receptor flexibility. Journal of Computational Chemistry 30(16): 2785-2791.
32. Pellegrini-Calace M, Maiwald T, Thornton JM (2009) PoreWalker: A novel tool for the identification and characterization of channels in transmembrane proteins from their three-dimensional structure. PLoS Computational Biology 5(7): e1000440.
33. Ramachandran GN, Ramakrishnan C, Sasisekharan V (1963) Stereochemistry of polypeptide chain configurations. Journal of Molecular Biology 7(1): 95-99.
34. Krieger E, Darden T, Nabuurs SB, et al. (2004) Making optimal use of empirical energy functions: Force-field parameterization in crystal space. Proteins: Structure, Function, and Bioinformatics 57(4): 678-683.

35. Singh UC, Kollman PA (1984) An approach to computing electrostatic charges for molecules. Journal of Computational Chemistry 5(2): 129-145.
36. Berendsen HJ, Postma JV, Van Gunsteren WF, et al. (1984) Molecular dynamics with coupling to an external bath. The Journal of Chemical Physics 81(8): 3684-3690.
37. Duan Y, Wu C, Chowdhury S, et al. (2003) A point-charge force field for molecular mechanics simulations of proteins based on condensed-phase quantum mechanical calculations. Journal of Computational Chemistry 24(16): 1999-2012.
38. Hiwase DK, Saunders V, Hewett D, et al. (2008) Dasatinib cellular uptake and efflux in chronic myeloid leukemia cells: Therapeutic implications. Clinical Cancer Research 14(12): 3881-3888.
39. Davies A, Jordanides NE, Giannoudis A, et al. (2009) Nilotinib concentration in cell lines and primary CD34+ chronic myeloid leukemia cells is not mediated by active uptake or efflux by major drug transporters. Leukemia 23(11): 1999-2006.
40. Mountford J, Davies A, Jordanides NE, et al. (2008) Nilotinib concentration in cell lines and CML CD34+ cells is not mediated by active uptake or efflux by major drug transporters. Blood 112(11): 3205.
41. Pedersen BP, Kumar H, Waight AB, et al. (2013) Crystal structure of a eukaryotic phosphate transporter. Nature 496(7446): 533-536.
42. Zhang X, Shirahatti NV, Mahadevan D, et al. (2005) A conserved glutamate residue in transmembrane helix 10 influences substrate specificity of rabbit OCT2 (SLC22A2). Journal of Biological Chemistry 280(41): 34813-34822.
43. Popp C, Gorboulev V, Müller TD, et al. (2005) Amino acids critical for substrate affinity of rat organic cation transporter 1 line the substrate binding region in a model derived from the tertiary structure of lactose permease. Molecular Pharmacology 67(5): 1600-1611.